Cell

Sensitizing Protective Tumor Microenvironments to Antibody-Mediated Therapy

Christian P. Pallasch,[1,2] Ilya Leskov,[1] Christian J. Braun,[1] Daniela Vorholt,[2] Adam Drake,[1] Yadira M. Soto-Feliciano,[1] Eric H. Bent,[1] Janine Schwamb,[2] Bettina Iliopoulou,[1] Nadine Kutsch,[2] Nico van Rooijen,[3] Lukas P. Frenzel,[2] Clemens M. Wendtner,[2] Lukas Heukamp,[4] Karl Anton Kreuzer,[2] Michael Hallek,[2] Jianzhu Chen,[1,*] and Michael T. Hemann[1,*]

[1]Koch Institute for Integrative Cancer Research and Department of Biology, Massachusetts Institute of Technology, Cambridge, MA 02139, USA

[2]Department of Internal Medicine, Center of Integrated Oncology, University of Cologne, Cologne 50931, Germany

[3]VFM Amsterdam 1081, Netherlands

[4]Department of Pathology, University Hospital of Cologne 50937, Germany

*Correspondence: jchen@mit.edu (J.C.), hemann@mit.edu (M.T.H.)

http://dx.doi.org/10.1016/j.cell.2013.12.041

SUMMARY

Therapy-resistant microenvironments represent a major barrier toward effective elimination of disseminated malignancies. Here, we show that select microenvironments can underlie resistance to antibody-based therapy. Using a humanized model of treatment refractory B cell leukemia, we find that infiltration of leukemia cells into the bone marrow rewires the tumor microenvironment to inhibit engulfment of antibody-targeted tumor cells. Resistance to macrophage-mediated killing can be overcome by combination regimens involving therapeutic antibodies and chemotherapy. Specifically, the nitrogen mustard cyclophosphamide induces an acute secretory activating phenotype (ASAP), releasing CCL4, IL8, VEGF, and TNFα from treated tumor cells. These factors induce macrophage infiltration and phagocytic activity in the bone marrow. Thus, the acute induction of stress-related cytokines can effectively target cancer cells for removal by the innate immune system. This synergistic chemoimmunotherapeutic regimen represents a potent strategy for using conventional anticancer agents to alter the tumor microenvironment and promote the efficacy of targeted therapeutics.

INTRODUCTION

While conventional chemotherapeutic agents have been successful in the treatment of many malignancies, recent advances in targeted molecular medicine used as a single agent or in combination with chemotherapeutic backbones have provided compelling breakthroughs in the treatment of drug refractory tumor types. Central among these advances has been the broad development of cancer-specific monoclonal antibodies and their adaptation for use in multiple malignancies. These antibodies have shown particular efficacy in the treatment of hematopoietic malignancies, where they have fundamentally altered the prognosis for numerous disease types (Dougan and Dranoff, 2009). The introduction of CD20-targeted therapy marked the beginning of the ''rituximab era'' in the treatment of B cell lymphomas (Molina, 2008). Chemoimmunotherapeutic regimens involving the addition of rituximab to established drug combinations have improved the long-term prognosis of non-Hodgkin Lymphoma (NHL) patients and have led to a significant reduction of overall NHL-related mortality (Coiffier et al., 2002) (Hallek et al., 2010). In addition to anti-CD20 antibodies, targeting CD52 has also provided a highly efficient consolidation treatment strategy for chronic lymphocytic leukemia (CLL) patients (Wendtner et al., 2004). However, despite the increasing use of antibody-based therapies in the clinic, the mechanisms underlying the efficacy of these agents, as well as the development of antibody resistance, remain unclear.

Therapeutic antibodies are generally thought to mediate their effects via direct antibody binding to target cells (Fan et al., 1993). In some cases, this binding may induce cell death by interfering with essential signaling pathways. Alternatively, therapeutic antibodies also mediate cell-nonautonomous killing, by complement binding and subsequent cytolysis. Finally, tumor cells can be effectively targeted through effector cell-mediated antibody-dependent cell-mediated cytotoxicity (ADCC) involving Fc-receptor-dependent recognition of antibody bound tumor cells by NK cells (Clynes et al., 2000) or macrophages (Minard-Colin et al., 2008). However, the evaluation of the relevant effector mechanisms of clinical grade therapeutic antibodies in vivo has been hampered by the lack of available animal models. Since therapeutic antibodies are generally human-specific, in vivo preclinical studies require the presentation of the human antigen on tumor cells (Sausville and Burger, 2006). Xenograft studies using human tumors are complicated by low engraftment rates and poor dissemination of engrafted tumor cells to autochthonous tumor microenvironments. With

the advent of humanized mouse models of cancer, it is now possible to reconstitute human organ systems and generate de novo arising tumors from modified human stem cells. These tumors develop in the appropriate microenvironment and harbor similar morphological and clinical characteristics as human disease. The development of human cancer cells in a relevant in vivo context allows one to investigate basic mechanisms concerning antibody-based therapies.

We recently developed a treatment refractory humanized mouse model of B cell lymphoma/leukemia amenable to treatment with therapeutic antibodies (Leskov et al., 2013). Here, by utilizing this humanized model, we identify the bone marrow as a treatment refractory niche and the leukemia-macrophage interaction as a decisive determinant of antibody-mediated toxicity. By examining the leukemia-macrophage cell interaction using targeted in vivo RNAi-screening and multiplex cytokine profiling, we identify factors secreted by treated leukemia cells that are major regulators of therapeutic response. In particular, we show an acute release of TNFα and VEGF specifically after cyclophosphamide (CTX) treatment from leukemia cells. Here, a strong synergy between CTX and therapeutic antibodies led to a curative treatment regimen in treatment refractory humanized mouse model of B cell lymphoma/leukemia, as well as in primary-patient-derived xenografts of B cell malignancies. These data suggest that models that can effectively interrogate the relevant mechanisms, and timing of antibody action can facilitate the development of curative therapeutic regimens from existing combinations of approved drugs.

RESULTS

Antibody-Mediated Tumor Cell Clearance Is Microenvironment Dependent

We recently generated a humanized mouse model of a highly chemoresistant B cell lymphoma/leukemia (Leskov et al., 2013). Specifically, B-cell-specific coexpression of the oncogenes c-Myc and Bcl-2 in mice reconstituted with human hematopoietic stem cells (HSCs) resulted in the rapid development of a disseminated and aggressive human malignancy (termed hMB) that effectively recapitulated the pathological and clinical characteristics of so-called "double-hit" lymphoma/leukemia. This constellation of genetic alterations, while rare, is associated with poor patient prognosis, with an average survival time of only 4–12 months following diagnosis (Aukema et al., 2011). Consistent with the human clinical data, leukemia-bearing mice were highly resistant to conventional chemotherapy. However, mice were transiently responsive to the anti-CD52 antibody alemtuzumab.

To investigate the mechanism of response and subsequent relapse on antibody-based therapy in this model, we examined the efficacy of alemtuzumab in distinct leukemia-bearing organ sites in secondary transplant recipients of hMB tumors (Figure 1A). Notably, while we observed a profound therapeutic response in the peripheral blood and spleen of recipients, tumor cells in the bone marrow were largely refractory to treatment (Figure 1B). This resistance was not due to impaired antibody binding, as use of a fluorescently labeled alemtuzumab showed antibody binding to the vast majority of tumor cells in this compartment in vivo (Figures S1A–S1C available online).

Antibody-Mediated Tumor Clearance Is Effector Cell Dependent

To determine the mechanism underlying the compartment-specific antibody response, we first examined the effector mechanisms contributing to leukemia cell clearance. Notably, response to alemtuzumab injection was not due to direct antitumor or complement-binding-dependent induction of cell death or apoptosis (Figure S1D). We next asked whether the cytotoxic effect of alemtuzumab in vivo requires the Fc portion of the antibody. We administered full-length alemtuzumab or alemtuzumab lacking its Fc portion (referred to as $F[ab]_2$) at equivalent doses into leukemia-bearing mice at the onset of disease manifestation. Relative to full-length alemtuzumab, which effectively reduced tumor burden in the spleen, the $F(ab')_2$ fragment of alemtuzumab failed to elicit any antitumor effect (Figure 1C). Given that full-length and the $F(ab')_2$ fragment of alemtuzumab have the same binding affinity to CD52, this result suggests that alemtuzumab efficacy is not due to direct binding to CD52. Rather, alemtuzumab's antitumor activity is mediated by recruiting effector cells that bear the Fc receptor (FcR).

Macrophage-Mediated Tumor Clearance

Macrophages are key FcR-bearing effector cells known to mediate antibody-directed processes in vivo (Jaiswal et al., 2010). To test whether macrophages mediate alemtuzumab's antitumor activity, we assessed survival of leukemia cells in coculture with macrophages harvested from the peritoneum of NSG mice. Survival of GFP^+ leukemia cells decreased significantly in a time-dependent manner when full-length alemtuzumab, but not its $F(ab')_2$ fragment, was present (Figure 1D). Additionally, depleting macrophages from NSG mice in vivo via intravenous injection of clodronate-containing liposomes abolished alemtuzumab's antitumor activity (Figure 1E; compare columns 2 and 4). Given the absence of NK cells in the NSG mice, these results strongly implicate macrophages as the effector cells that mediate the antitumor effect of alemtuzumab in this model.

Following activation, macrophages employ multiple strategies to eliminate targets, including the generation of reactive oxygen species and nitric oxide, the release of cytokines that engage an inflammatory response and the direct phagocytosis of target cells or pathogens. To elucidate the precise mechanism of anti-CD52 antibody-mediated leukemia cell killing by macrophages, we first examined whether reactive oxygen species release from myeloid cells is induced by recognition of alemtuzumab-bound target cells. Specifically, we assessed the ability of bone-marrow-derived macrophages from either wild-type or $p47^{-/-}$ mice, which lack the ability to produce reactive oxygen species (ROS), to kill antibody bound tumor cells (Jackson et al., 1995). Here, we observed no difference between *NSG*, *C57BL6* $p47^{wt}$ and $p47^{-/-}$-derived macrophages (Figure S1E), suggesting a ROS-independent cytotoxicity.

To determine whether macrophages directly engulf and digest antibody-bound target cells, we performed a leukemia/macrophage coculture assay in the presence or absence of

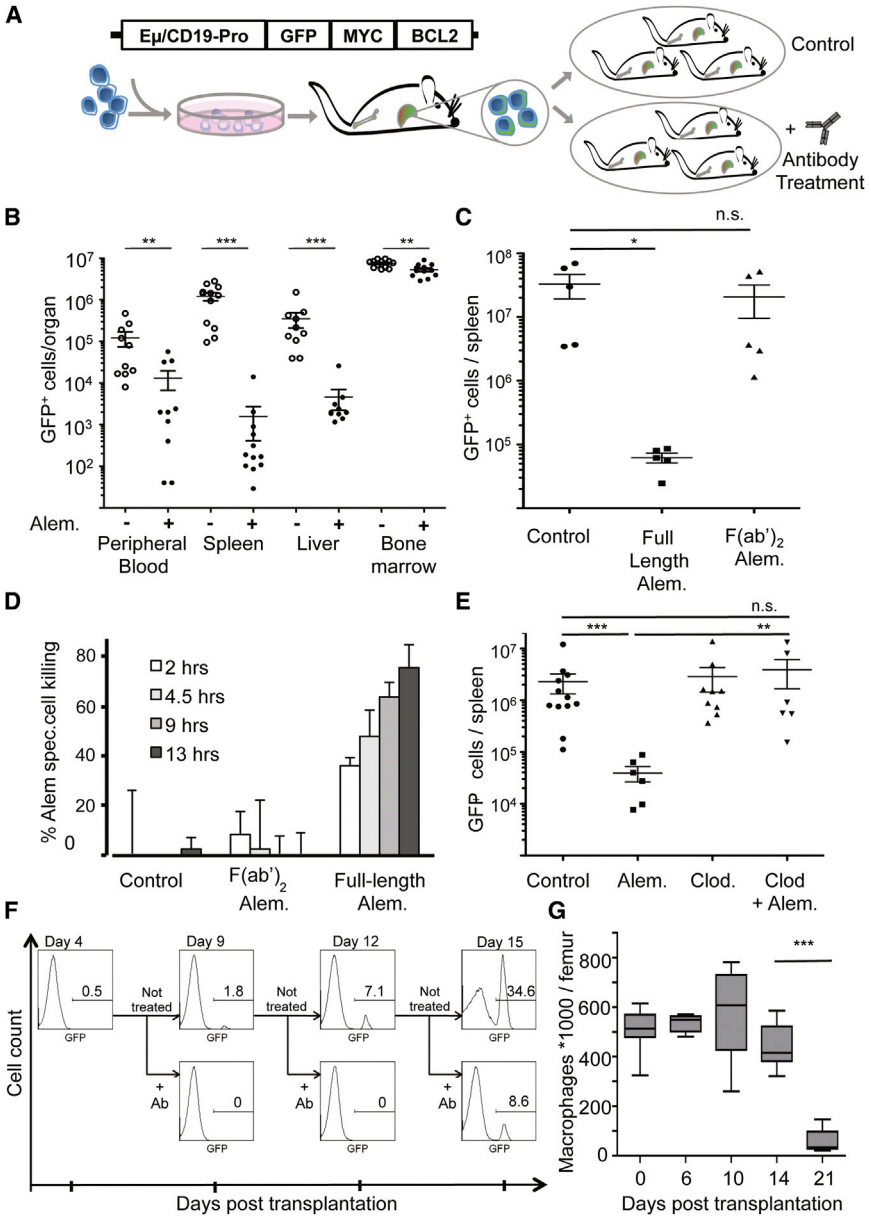

Figure 1. The Bone Marrow Provides a Resistant Niche That Protects Leukemia Cells from Antibody-Directed Macrophage Engulfment

(A) A schematic of the humanized hMB-model of double-hit lymphoma. Cord-blood-derived HSCs are infected with a B cell directed BCL2/MYC overexpressing construct. Primary leukemias are transplanted to secondary recipient mice for further treatment studies.

(B) A graph showing the relative tumor burden in distinct organs 8 days after initiating alemtuzumab treatment. Each symbol represents one mouse. For bone marrow, the total number of tumor cells in both femurs and tibias was counted.

(C) A graph comparing the antitumor effect of the full-length and the $F(ab')_2$ fragment of alemtuzumab in NSG mice after 7 days of treatment. Each symbol represents one mouse.

(D) A graph showing the relative macrophage-dependent cell death in the presence or absence of antibody.

(E) A graph showing the relative tumor cell number following treatment with or without clodronate and alemtuzumab. GFP^+ leukemic cells in the spleen were quantified after 7 days of treatment.

(F) Histograms showing the percentage of $hCD45^+$/ GFP^+ cells in the bone marrow. Secondary hMB recipient mice were treated at the indicated times after leukemia cell transplantation, and the presence of GFP^+ leukemic cells was assayed on day 9, 12, or 15, respectively.

(G) A graph showing the time-dependent abundance of $CD11b^+/GR1^{lo}/CD11c^-/F4/80^+$ macrophages in femurs of hMB mice by flow cytometry.

For all bar graphs, average and SEM are shown (* = $p < 0.05$, ** = $p < 0.01$, and *** = $p < 0.001$). See also Figure S1 and Movie S1.

alemtuzumab. We then assessed the extent of macrophage-mediated phagocytosis of tumor cells by live cell imaging. Here, we observed direct engulfment of malignant cells by macrophages, starting within minutes of antibody addition to the cocultured cells. Macrophages displayed varying propensity to engulf leukemic cells, ranging from 1 to 5 tumor cells per macrophage. These data suggest that antibody-mediated macrophage phagocytosis is the major mechanism of alemtuzumab-dependent cellular cytotoxicity (Movie S1).

To specifically address if resistance to antibody treatment is inherently present in the bone marrow microenvironment or if disease progression induces a treatment refractory microenvironment, we assessed treatment response at very early time points in disease progression. Specifically, we administered the antibody at 4, 9, 12, and 15 days after leukemic cell transplantation into secondary recipients. When mice were treated with alemtuzumab 4 days after transplantation, at a time when leukemic cells were not detectable in the peripheral blood, no leukemic cells were subsequently detected in the bone marrow at day 9, whereas vehicle-treated control mice showed clear disease progression (Figure 1F). Similarly, when mice were treated 9 days after transplantation, no leukemic cells were detected in the bone marrow at day 12. However, when mice were treated at 12 days posttransplantation, surviving leukemic cells were readily detected in the bone marrow at day 15. When monitoring the macrophage frequency in the bone marrow during progression of the disease, total macrophage numbers remained stable until day 14, with a rapid decline once leukemic cells prevented hematopoiesis in the bone marrow at day 21 (Figure 1G). Assuming the progressive expansion of cells in the bone marrow from day 4 to day 12, these data suggest that alemtuzumab resistance develops, in part, as the leukemic cells grow and overtake the bone marrow.

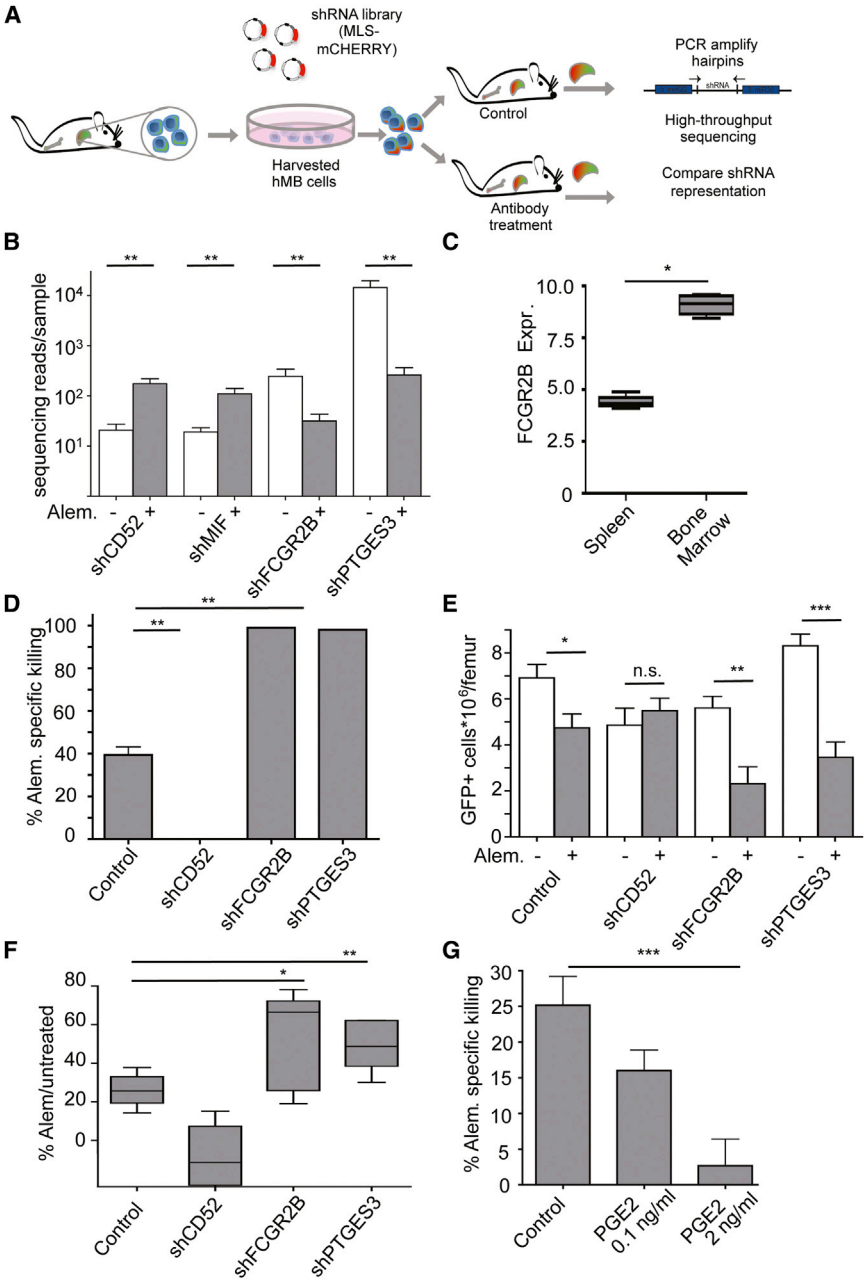

Figure 2. In Vivo RNAi-Screening Identifies PGE2 and FCGR2B-Mediated Resistance to Alemtuzumab

(A) Schematic of the shRNA screening approach. Primary hMB mouse-derived leukemia cells were infected with an shRNA pool ex vivo and mCherry$^+$ sorted cells were transplanted to secondary recipient mice. Prior and subsequent to treatment, leukemia cells were isolated and subjected to shRNA sequencing.

(B) A bar graph showing the distribution of shRNA representation in untreated control samples (n = 9) versus alemtuzumab-treated mice (n = 9).

(C) A graph showing the relative expression of FCGR2B in spleen versus bone-marrow-derived leukemic cells, as determined by flow cytometry. Data are displayed as the ratio of the mean fluorescence intensity in specific stain/isotype control (n = 4).

(D) A bar graph showing the effects of specific shRNA-mediated knockdown on macrophage killing in vitro. The percentage of antibody-mediated killing in by macrophage ADCC was calculated from absolute counts of GFP$^+$ cells. Percent killing = %100 − (100*($N^{treated}$/$N^{untreated}$)) (n = 8 per group).

(E) A bar graph showing the treatment response shRNA-infected leukemias to alemtuzumab in vivo. Disease burden was assessed by flow cytometry and shown as absolute counts of leukemic cells per femur in untreated versus antibody-treated mice.

(F) A bar graph comparing the percentage (referring to absolute counts displayed in D) of residual disease in shRNA-infected leukemias after antibody treatment (n = 6 per group).

(G) A bar graph showing the effect of PGE2 on macrophage mediated ADCC of leukemia cells. For all bar graphs, average and SEM are shown (* = $p < 0.05$, ** = $p < 0.01$, and *** = $p < 0.001$). See also Figure S2 and Table S1.

Macrophage-Dependent Therapeutic Response Is Dependent on Tumor Cell Surface Receptors and Secretory Phenotypes

In order to identify factors governing resistance or susceptibility of tumor cells to alemtuzumab-mediated clearance, we performed a targeted shRNA screen in vivo (Figure 2A). A focused miR-30-based shRNA library was generated toward 19 human genes implicated in macrophage phagocytic activity or therapeutic antibody efficacy (Table S1) (Meacham et al., 2009). As a positive control, CD52-specific shRNAs were included. At day 21 posttransplantation when leukemic cells were detected in the peripheral blood, recipient mice were separated into an untreated control group (n = 10) and an alemtuzumab treatment group (n = 10). shRNA representation was quantified in the leukemia cell population in control mice at day 21 posttransplantation and at leukemia relapse following antibody administration in alemtuzumab-treated mice (Figure 2A and Table S1). Comparing shRNA representation in the presence and absence of therapy, we identified two independent shRNAs targeting CD52 enriched in leukemia cell populations derived from alemtuzumab-treated mice. In contrast, shRNAs targeting Fc-gamma receptor 2B and prostaglandin synthetase 3 were depleted in alemtuzumab-treated mice (Figure 2B). Since alemtuzumab response is significantly impaired in bone-marrow residing cells, we suspected that context-dependent expression differences in resistance factors identified by RNAi might represent an underlying cause of resistance. Consistent with this idea, FCGR2B expression was significantly higher on tumor cells in the bone marrow relative to the spleen (Figure 2C).

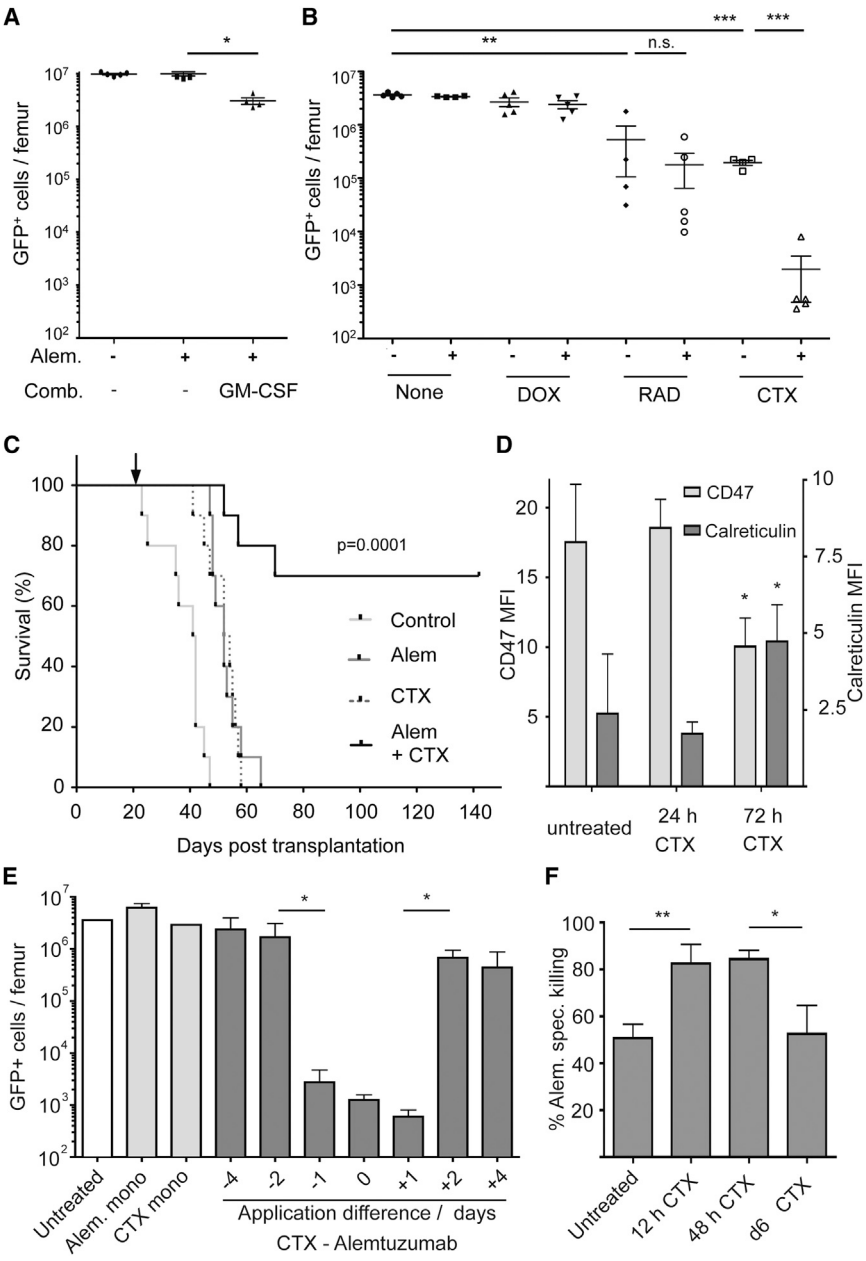

Figure 3. Combination Therapy with Alemtuzumab and CTX Cures Pre-B-ALL in the hMB Model

(A and B) A graph showing the number of live tumor cells in the bone marrow of mice treated with alemtuzumab alone or in combination with (A) GM-CSF (2 × 100 ng/dose s.c. for 6 days) or (B) doxorubicin (5 mg/kg) (DOX), CTX (100 mg/kg) (CTX), or whole-body irradiation (5 Gy) (RAD). Organs were harvested 8 days after treatment initiation. Each symbol represents one mouse.

(C) Kaplan-Meier analysis comparing the survival of secondary hMB recipient mice receiving different antitumor treatments as indicated by arrow (n = 10 per treatment arm).

(D) A graph displaying CD47 and calreticulin expression on leukemia cells prior to CTX treatment and 24 and 72 hr posttreatment posttreatment.

(E) A graph showing the number of surviving GFP$^+$ cells following treatment of mice with alemtuzumab at distinct intervals relative to CTX.

(F) A graph showing susceptibility to macrophage-mediated killing of hMB cells ex vivo following CTX chemotherapy. Data are shown at 12 hr, 48 hr and after 6 days. For all bar graphs, average and SEM are shown (* = $p < 0.05$, ** = $p < 0.01$, and *** = $p < 0.001$).

See also Figures S3 and S4.

In order to validate the in vivo RNAi screening results, we examined the influence of leukemia cell secreted factors on alemtuzumab-dependent macrophage-mediated phagocytosis of tumor cells in vitro. As expected, shCD52-infected leukemia cells were entirely resistant to alemtuzumab-mediated phagocytosis. In contrast, shRNAs targeting the cytosolic prostaglandin synthetase 3 (PTGES3) and the Fc receptor 2B (FCGR2B) significantly enhanced alemtuzumab-mediated depletion of malignant cells in vitro (Figure 2D). Injecting pure shRNA-infected hMB cells to validate therapeutic response in vivo revealed an impaired response to therapy in the shCD52-positive control, while FCGR2B and PTGES3 knockdown leukemia cells showed improved therapeutic response in the bone marrow compared to control vector-infected leukemias (Figures 2E and 2F, and Figure S2). Moreover, PGE2 as the terminal effector of PTGES3 activity significantly inhibited phagocytosis of leukemia cells in a dose-dependent manner (Figure 2G). Thus, a PGE2 secretory response and FCGR2B-mediated binding competition contribute to development of an antibody refractory microenvironment in the bone marrow.

Sensitizing Drug-Resistant Tumor Cells to Antibody-Mediated Clearance

Given the primary role of macrophages in antibody-mediated antitumor activity in this context, we sought to enhance effector cell responses in the bone marrow. First, we pretreated leukemia-bearing mice with GM-CSF, which stimulates myelopoiesis and macrophage differentiation. Although this approach improved the efficacy of alemtuzumab by ~3-fold (Figure 3A), it only resulted in a mild reduction in the tumor load in the bone marrow. Similarly, combining alemtuzumab with doxorubicin (5 mg/kg) failed to significantly improve the efficacy of alemtuzumab in the bone marrow (Figure 3B), and whole-body irradiation (5 Gy) had only a mild additive effect when combined with alemtuzumab. In contrast, the combination of alemtuzumab and CTX (300 mg/kg) yielded a strikingly synergistic therapeutic effect, leading to near-complete elimination of disease in the bone

marrow (Figure 3B). Alemtuzumab or CTX alone reduced tumor burden in the bone marrow 5- and 10-fold, respectively (Figures 1B and 3B). Thus, their additive effect in the bone marrow was expected to result in ~~20% residual malignancy. The observed 0.013% residual disease reflects a level of synergy that is approximately 160-fold higher than expected. Furthermore, we could systematically reduce our initial CTX dose of 300 mg/kg to a minimal dose of 100 mg/kg and still maintain comparable drug synergy (Figure S3A), suggesting that the levels of DNA damage induced by the alkylating activity of CTX may not account for its entire antitumor activity. Notably, unlike leukemia-bearing mice treated with either alemtuzumab or CTX alone, which survived on average 10 days longer than untreated hMB mice, most hMB mice treated with a combination of CTX and alemtuzumab showed a complete and durable response to therapy— with most still alive >6 months after their initial reconstitution with leukemic cells (Figure 3C). During this period, no residual tumor cells were detected in the peripheral blood of the surviving mice (Figure S3B). Moreover, the few mice that died following combination therapy also failed to show any evidence of leukemia, suggesting their death was due to therapeutic toxicity. The synergy of alemtuzumab and CTX was very specific to this drug combination, as codosing alemtuzumab with Ara-C, chlorambucil, or bendamustine failed to produce a synergistic effect (Figure S3C).

To identify the mechanism by which CTX treatment promotes alemtuzumab efficacy in the bone marrow, we first examined the status of genes identified as promoting antibody resistance in our targeted RNAi screen. While FCGR2B expression was not altered in response to chemotherapy, CTX treatment significantly reduced PGE2 levels in bone-marrow-derived leukemia cells (Figure S4A). Given this change in PGE2 expression, we were interested in determining whether CTX mediates additional "macrophage-relevant" changes in leukemia cells. For example, cell surface expression of CD47 has recently been shown to be a key regulator of macrophage-mediated engulfment of tumor cells (Chao et al., 2011; Chao et al., 2010). Cell surface staining for the antiphagocytic factor CD47 showed a significant downregulation of this protein on leukemia cells 72 hr post-CTX dosing. In contrast, the prophagocytic factor calreticulin was induced 72 hr post-CTX therapy (Figure 3D), and this was associated with increased XBP-1 splicing, indicative of elevated ER stress (Figure S4B). Finally, senescence-associated β-galactosidase activity was first detected in leukemia cells 6 days following CTX treatment (Figure S4C).

Since a number of these CTX-induced changes in leukemia cells occur only after several days, we next examined the temporal dynamics of synergy following CTX treatment. Leukemia-bearing mice were injected with cyclophosphamide at treatment day 0—corresponding to day 21 postleukemia cell transplantation. In order to identify the optimal time point for combinatorial treatment with alemtuzumab, the antibody was applied at days −4, −2, −1, 0, 1, 2, and 4 relative to CTX application. Synergistic elimination of leukemia cells in the bone marrow was seen only from day −1 to day 1 of antibody application. Thus, the synergy of antibody and CTX treatment is limited to a short time frame (Figure 3E). Notably, when comparing antibody-mediated phagocytosis of bone-marrow-derived leukemic cells isolated after 12 hr, 48 hr, and 6 days post-CTX treatment in vitro, peak levels of phagocytosis were seen in cells isolated shortly after 12 hr or 48 hr posttreatment (Figure 3F). However, phagocytosis of tumor cells from mice 6 days post-CTX treatment returned to the baseline level of engulfment of untreated cells. Thus, CTX treatment alters the abundance and functionality of macrophages in a rapid, but transient, time window during combination therapy.

A Drug-Induced Secretory Response Promotes Macrophage Antitumor Activity

Recruitment of macrophages to CTX-treated bone marrow might involve global changes in the bone marrow microenvironment that increase general effector cell accessibility, or, alternatively, the release of factors from tumor cells that promote macrophage recruitment or activity. To differentiate between these hypotheses, we isolated leukemia cells from bone marrow and spleens of mock-treated or CTX-treated leukemia-bearing mice 24 hr after treatment. Here, 10^5 untreated or treated leukemia cells were cocultured with macrophages in the presence of alemtuzumab. Untreated bone-marrow-derived tumor cells were significantly less susceptible to macrophage-mediated killing. Interestingly, CTX treatment significantly improved phagocytosis of leukemia cells—to a level equivalent with spleen-derived hMB cells. Furthermore, spleen-derived leukemia cells could be further primed for macrophage-mediated killing by CTX treatment (Figure 4A).

Since tumor cell secretory mechanisms were identified as central to tumor cell clearance by macrophages in our initial in vivo RNAi screen, we examined cytokine secretion upon cytotoxic treatment of leukemia cells in the bone marrow. Specifically, we generated conditioned media from leukemia cells isolated from the bone marrow following CTX treatment. We then exposed thioglycollate-induced macrophages to the conditioned media in the presence of alemtuzumab and untreated leukemia cells. The treated bone-marrow-conditioned media significantly enhanced phagocytic activity compared to either control media or conditioned media from untreated bone marrow (Figure 4B). Since PGE2 levels were significantly reduced in conditioned media obtained from CTX-pretreated bone-marrow-derived hMB cells, we analyzed the effects of adding back PGE2 to the conditioned media from CTX-pretreated leukemia cells. Here, we could completely abrogate the stimulatory effects of CTX with a low dose of 1 ng/ml of PGE2 (Figure 4C).

In order to identify specific factors responsible for the prophagocytic secretory state of CTX-treated tumor cells, we applied samples from treated bone-marrow-derived leukemia cells to a human 65-cytokine Bio-Plex assay. Both irradiation and CTX significantly induced a variety of cytokines in the bone marrow (Table S2). However, several factors were induced exclusively by CTX. Specifically, we observed acute induction of IL8, TNFα, VEGF, and CCL4 only in the presence of CTX (Figure 4D). We next added the clinical grade blocking antibodies infliximab and bevacizumab, specific for TNFα and VEGF, respectively, to conditioned media prior to the phagocytosis assay. Specific blockade of TNF and VEGF revealed a significant abrogation of the prophagocytic properties of conditioned media

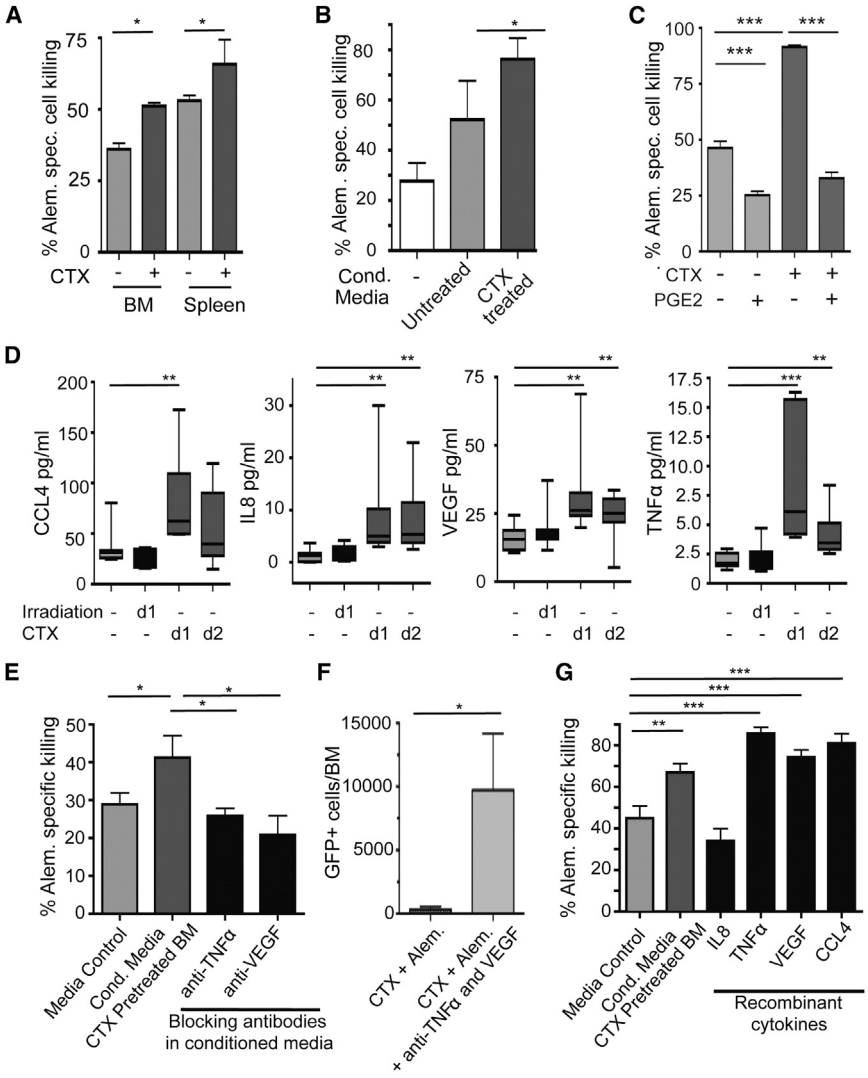

Figure 4. CTX/Alemtuzumab Synergy Is Mediated by an Acute Secretory Response from Treated Leukemia Cells

(A) A bar graph showing the level of antibody-mediated cell death of bone marrow and spleen leukemia cells from hMB leukemia mice following treatment with 100 mg/kg CTX in the presence of peritoneal macrophages.

(B) A bar graph showing the level of alemtuzumab-mediated ADCC 1 day after exposure to conditioned media from the bone marrow of CTX-treated mice or untreated controls.

(C) A bar graph showing the level of alemtuzumab-mediated ADCC following the addition of 1 ng/ml PGE2 to the conditioned media from CTX or control pretreated leukemia cells.

(D) Quantification of cytokine secretion from bone marrow residing leukemia cells following irradiation (5 Gy) or CTX (100 mg/kg). Lysates from whole-tibia bone marrow from leukemic mice were subject to a human cytokine bioplex assay.

(E) A bar graph showing the level of ADCC following prior incubation of CTX-conditioned media with the indicated cytokine-specific blocking antibodies.

(F) A bar graph showing the number of surviving cells in vivo in the bone marrow following treatment with CTX and alemtuzumab plus or minus the blocking TNF and VEGF antibodies infliximab and bevacizumab.

(G) A graph showing the effect of the indicated recombinant human cytokines (100 ng/ml each) on alemtuzumab-mediated ADCC. All macrophage ADCC assays were performed using 10 individual hMB cell lines. For all bar graphs, average and SEM are shown (* = $p < 0.05$, ** = $p < 0.01$ and *** = $p < 0.001$).

See also Table S2.

(Figure 4E). Blocking TNF and VEGF with infliximab and bevacizumab in vivo also significantly reduced the efficiency of CTX/alemtuzumab treatment (Figure 4F). Additionally, recombinant TNFα, CCL4 and VEGF significantly improved phagocytic activity—at a dose range similar to that induced by conditioned media from CTX-pretreated leukemic bone marrow (Figure 4G). Thus, the acute secretory response, as opposed to later occurring leukemia cell surface alterations, plays the predominant role in macrophage activation following CTX treatment.

CTX-Induced Changes in the Tumor Microenvironment

We next analyzed downstream effects of the CTX-induced secretory response on the tumor microenvironment. Here, we specifically focused on the quantity and differentiation status of macrophages, as they represent the main effector cells of alemtuzumab therapy. First, we quantified bone marrow macrophage content by flow cytometry prior and subsequent to treatment. CTX promoted a progressive increase in the concentration of CD11b$^+$/Gr-1^{lo}/CD11c$^-$/F4/80$^+$ bone marrow macrophages, evident as early as 24 hr after treatment initiation (Figure 5A). To more directly assess phagocytic activity in vivo, we injected 70 kD Dextran-Texas Red particles intravenous. into CTX-treated mice and untreated controls. Examination of the bone marrow and spleen by multiphoton confocal microscopy for Texas-Red-positive macrophages (indicating particle phagocytosis) showed dramatically increased numbers of Texas-Red-positive cells at day 5 after CTX treatment—with macrophage densities reaching those equivalent to spleen (Figures 5B–5D). Histopathology of CTX-treated mice revealed partially restored hematopoiesis in the spleen and bone marrow at day 7 post-treatment (Figure S4C). However, numerous blastoid cells were still present, consistent with the partial response to CTX monotherapy shown by flow cytometry (Figure 3B).

Macrophages can be induced to differentiate into distinct functional states—a process operationally defined as M1-M2 polarization. To examine changes in macrophage function induced by either disease progression or treatment, we performed a multiplex flow cytometry analysis of F4/80$^+$/Gr-1lo bone marrow and spleen cell populations using macrophage differentiation markers. Leukemic infiltration significantly induced

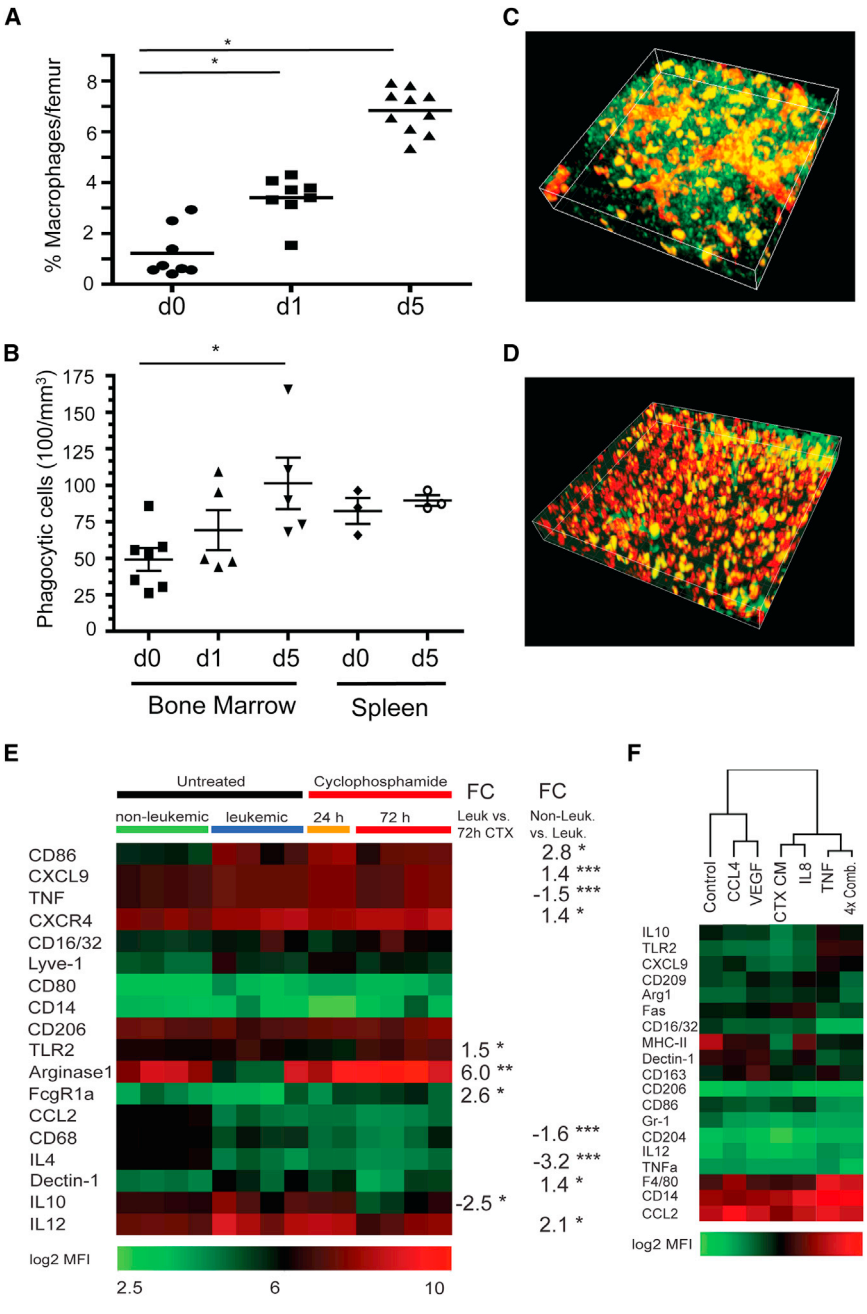

Figure 5. CTX Increases Macrophage Frequency and Shows Time-Dependent Synergy with Antibody Therapy

(A) Flow cytometry quantification of the number of bone marrow macrophages after CTX treatment, as assessed by $CD11b^{+}/GR1^{lo}/CD11c^{-}/F4/80^{+}$ staining.

(B) A graph showing the number of phagocytic cells in the bone marrow following treatment with 100 mg/kg CTX. Phagocytic cells were quantified by automated identification of Texas-Red-positive cells using IMARIS software package.

(C and D) Representative three-dimensional reconstruction of (C) untreated bone marrow and (D) bone marrow 5 days post-CTX treatment. Green cells indicate leukemic GFP^{+} cells, while phagocytic cells harboring dextran-Texas Red uptake are displayed in red (* = $p < 0.05$). See also Figure S4.

(E) A heat map showing macrophage marker expression, expressed as mean fluorescence intensities (MFIs), from control (nonleukemic) mice, untreated leukemic mice and CTX-treated leukemic mice (24 hr and 72 hr post-treatment onset). Significant changes in marker expression are indicated to the right of the heat map.

(F) A heat map showing marker expression in peritoneal macrophages cultivated in the presence of conditioned media generated from CTX-treated leukemia cells, recombinant CCL4, VEGF, TNFα, or IL8 or a combination of all 4 recombinant factors. Marker expression was obtained by flow cytometry and displayed as MFIs. Clustering of experimental conditions was performed using a Pearson correlation (* = $p < 0.05$, ** = $p < 0.01$ and *** = $p < 0.001$).

the expression of CD86, CXCL9, CXCR4, Dectin-1, and Il12, while decreasing levels of TNFα, CD68, and IL4 (Figure 5E). These changes reflect a loss of macrophage effector function during leukemia progression, as they reveal a differentiation state distinct from both the naive macrophage and the classic M1-M2 polarized states. Conversely, CTX treatment of leukemic mice significantly induced expression of TLR2, Arginase-1, and Fcgr1α, while decreasing IL10 levels—changes consistent with macrophage activation.

To further characterize the effects of the CTX-induced leukemia secretory response on macrophages, we compared macrophage status in vitro upon incubation for 3 days in conditioned media from treated leukemia cells versus that induced by recombinant cytokines (Figure 5F). Hierarchical clustering of the relative expression of a 20-marker panel of macrophage differentiation markers revealed that the addition of IL8 and TNFα or the combination of CCL4, VEGF, TNFα, and IL8 most closely mimicked the changes induced by CTX-conditioned media.

Chemoimmunotherapeutic Synergy Is Independent of Genetic Background and Effector Cell Type

To determine whether the CTX-induced secretory response is common to distinct leukemias in fully immunocompetent settings, we treated mice bearing a murine *BCR-ABL*$^{+}$ B-ALL. Treatment of these mice with CTX revealed a similar sensitization to a mouse-specific anti-CD20 therapeutic antibody (clone 18B12) (Figure 6A). Conditioned media generated from

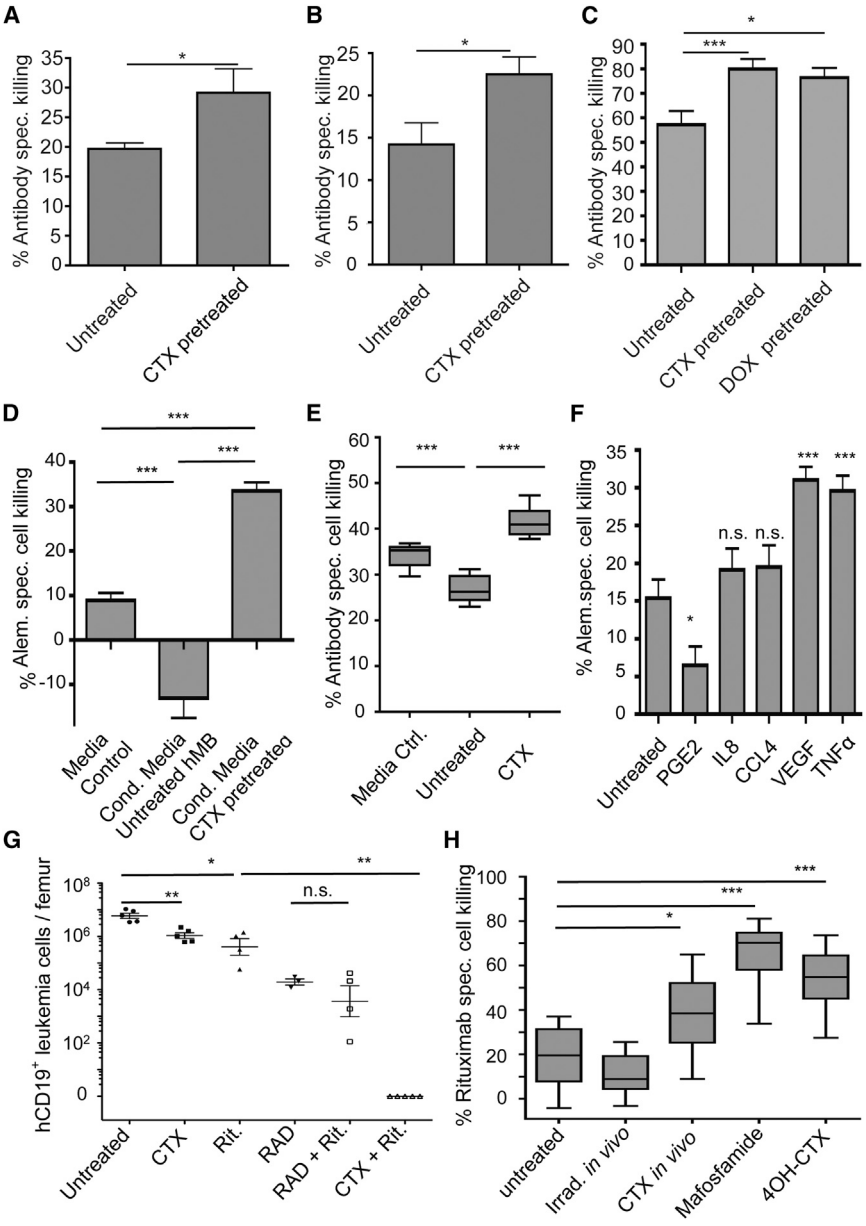

Figure 6. CTX-Dependent Secretory Responses Can Be Elicited in Independent Murine Tumor Models, Patient-Derived Cells and Independent Effector Cells

(A) A bar graph showing macrophage-dependent phagocytosis of in vivo CTX treated murine $Arf^{-/-}Ph^{+}$ B-ALL in the absence or presence of the 18B12 anti-CD20 antibody.

(B) A bar graph showing the effect of conditioned media generated from cells derived from untreated versus CTX-treated $Arf^{-/-}Ph^{+}$ B-ALL-bearing mice on alemtuzumab-dependent phagocytosis of hMB cells.

(C) A graph showing the effect of conditioned media generated from cells derived from untreated or DOX- or CTX-treated *Eμ-Myc* $/Arf^{-/-}$ lymphoma-bearing mice on alemtuzumab-dependent phagocytosis of hMB cells.

(D) A graph showing the relative level of alemtuzumab-mediated cell killing by human primary monocytes in the presence of conditioned media derived from control or CTX-treated leukemia cells.

(E) A graph showing the level of alemtuzumab-mediated leukemia cell lysis, as determined by a europium-release assay, using primary human NK-cells from healthy donors.

(F) A bar graph showing the level of human monocyte ADCC in the presence of PGE2, IL8, CCL4, VEGF, and TNFα.

(G) A graph showing the response of patient-derived B-ALL xenografts in NSG mice to treatment with rituximab (3× 10 mg/kg), total body irradiation (5Gy) CTX (2× 100 mg/kg), or their respective combinations, as indicated.

(H) A graph showing the level of rituximab-mediated ADCC following exposure of leukemia cells to conditioned media generated from tumor cells isolated from untreated, irradiated (5 Gy) and CTX-treated (100 mg/kg) primary human patient B-ALL xenografted mice. Mafosfamide and 4-OH-CTX were used to treat cells ex vivo for 6 hr, and conditioned media was obtained after 24 hr of subsequent culture. Untreated leukemia cells served as target cells for Rituximab-mediated ADCC. For all graphs, * = $p < 0.05$, ** = $p < 0.01$ and *** = $p < 0.001$.

CTX-pretreated versus untreated mice displayed a similar activation of phagocytosis by macrophages, using hMB cells as target cells (Figure 6B). Finally, we analyzed a third model of B cell malignancy, the *Eμ-Myc* model of Burkitt's lymphoma. Conditioned media from lymphomas treated with CTX in vivo induced a highly significant increase in the phagocytosis of antibody-targeted cells, although a moderate increase was also seen in this context in the presence of conditioned media from doxorubicin-treated cells (Figure 6C).

Antibody-Directed Tumor Cell Engulfment Occurs Similarly in the Presence of Human Macrophages

To examine whether these findings could be extended to human effector cells, we introduced human monocytes from healthy donors into our ADCC assay. In the presence of conditioned media from CTX-pretreated leukemia cells, human monocytes showed significantly higher ADCC compared to media control. Notably, conditioned media from untreated leukemias actually improved leukemia cell survival in vitro in the presence of monocytes and therapeutic antibody (Figure 6D)—highlighting the importance of CTX treatment in supporting antibody efficacy. Additionally, we examined human primary NK cells as another clinically relevant effector cell subpopulation to determine NK-cell-mediated ADCC in the context of chemotherapy. Preincubation of NK cells with conditioned media from either untreated or CTX-treated leukemia cells revealed significantly higher antibody-specific leukemia cell lysis in the context CTX-induced ASAP (Figure 6E). Finally, the inhibitory effect of PGE2

on ADCC was also observed in this setting, as was improved leukemia cell killing in the presence of recombinant VEGF and TNFα (Figure 6F). This improved leukemia cell killing was also seen upon dose reduction of VEGF (Figure S5A), suggesting that ADCC can be effectively promoted at physiologically relevant doses of paracrine signaling molecules.

We next sought to determine whether these findings were broadly applicable to other therapeutic antibodies and to patient-derived leukemia models. Specifically, we examined regimens involving the anti-CD20 antibody rituximab. Rituximab is currently a key component of numerous drug regimens targeting B cell malignancies. To generate a drug-resistant xenograft model of ALL, we injected 10^7 Ph^+ $CD20^+$ ALL cells into sublethally irradiated (2.5 Gy) NRG mice (Figure S5B). After 10 to 16 weeks, mice showed leukemic disease involving spleen with pronounced splenomegaly and infiltration into the bone marrow, as previously described (Meyer et al., 2011). Engrafted leukemia cells were isolated from spleens and 10^7 cells were engrafted into secondary recipient mice. Leukemia-bearing recipient mice were treated with 2× treatment cycles at days 1 and 7 (100 mg/kg CTX/5 Gy/20 mg/kg Rituximab). Interestingly, resistance to antibody monotherapy in the bone marrow was recapitulated in the human-patient-derived xenograft model. Additionally, similar to our hMB humanized mouse model of leukemia, we detected a partial response to single-agent treatments. For example, additive, but not synergistic, effects were observed after combining rituximab and irradiation. However, the combination of CTX with rituximab completely eradicated the leukemic cell infiltration (Figure 6G).

To determine whether drug-induced secretory responses were relevant to antibody-induced phagocytosis of patient-derived tumors, we generated conditioned media from irradiated and CTX-treated primary human *BCR-ABL*$^+$ B-ALL patient-derived cells. Additionally, untreated *BCR-ABL*$^+$ B-ALL cell were treated ex vivo with sublethal drug doses of mafosfamide (20 μM) and 4-OH- CTX. Conditioned media were then used in macrophage coculture treatment experiments targeting primary patient-derived ALL cells. Rituximab induced approximately 20% B-ALL cell killing in untreated control media, while no enhancement of rituximab-mediated killing could be observed in conditioned media generated from irradiated mice. However, conditioned media generated from leukemia cells following CTX treatment in vivo significantly enhanced rituximab-mediated killing. Furthermore, conditioned media from ex vivo treatment with CTX proxies mafosfamide and 4-OH-CTX could also significantly enhance rituximab-mediated depletion of ALL cells (Figure 6H). Thus, we could recapitulate findings from the humanized leukemia mouse model utilizing independent effector cells, multiple therapeutic antibodies and genetically distinct patient samples from independent clinical entities. In all cases, we observed strong chemoimmunotherapeutic synergy, mediated by a CTX-induced activation of effector cells.

Chemotherapy Induces Macrophage Infiltration to Bone Marrow in ALL Patients

While we observed acute cytokine release and macrophage activation in patient-cell-derived xenograft models, we sought to assess the impact of chemotherapy on ALL microenvironments in a clinical context. First, we analyzed serum cytokine concentrations in patients undergoing treatment (Table S3). While we could show increased TNFα in ALL patient sera prior to therapy compared to normal controls (Figure S6), we detected lower levels after treatment onset, most likely related to the standardized multimodal treatment containing high-dosage dexamethasone. However, when we assessed bone marrow aspirates of six ALL patients taken prior to and following CTX-containing therapy (Gökbuget et al., 2004), we observed a significant increase in the macrophage population in the bone marrow as demonstrated by flow cytometry assessment of macrophage markers CD13, CD14, and CD33 (Figure 7A) and CD68-immunostaining of bone marrow smears (Figures 7B and 7C). Thus, similar to our mouse models, we see an accumulation of macrophages in treatment-refractory tumor microenvironments of leukemia patients undergoing CTX-containing treatment regimens.

DISCUSSION

Here, we sought to identify effector mechanisms and strategies to overcome resistance to antibody-based therapies in a humanized mouse model of acute lymphoblastic leukemia. Notably, we identified macrophages as the central mediators of this antibody-based antileukemic response in vivo. Recent studies of tumor-macrophage interaction have described enhanced growth and metastasis (and drug resistance) following macrophage infiltration in breast cancer (Chen et al., 2011; DeNardo et al., 2009; DeNardo et al., 2011). We observed a critical antitumorigenic role for macrophages following administration of therapeutic antibodies in blood cancers, suggesting that this dynamic cell type has context-specific roles during tumor progression and response to therapy.

The therapeutic response to antibody application was strongly dependent upon the tumor microenvironment, a feature that is mirrored by the primary alemtuzumab resistance observed in bulky disease in chronic lymphocytic leukemia (Moreton and Hillmen, 2003). While an effective antitumor response was observed in the spleen, low macrophage frequency led to a poor response in the bone marrow. By performing targeted in vivo RNAi screening, we identified Fc-gamma receptor 2B expression and PGE2 as key determinants of the response to antibody treatment. FCGR2B has previously been shown to interfere with rituximab-mediated ADCC of leukemia cells in vitro (Lim et al., 2011). Since FCGR2B displays higher expression at the site of primary resistance in the bone marrow, FCGR2B levels may contribute to the differential response to antibodies in distinct organ sites. PGE2 release is strongly suppressed in CTX-treated leukemic cells. PGE2 release is also prevalent in other malignancies, where its immunosuppressive properties lead to T cell and APC inactivation and cancer progression (Harris et al., 2002; Williams et al., 2000). Finally, PGE2 is involved in the release of TNFα and VEGF (Shinomiya et al., 2001; Williams et al., 2000), factors that represent major determinants of the acute secretory response described in this study.

The Mechanism of Macrophage Activation by CTX

The use of a humanized leukemia mouse model allowed us to model the emerging clinical practice of combining front-line

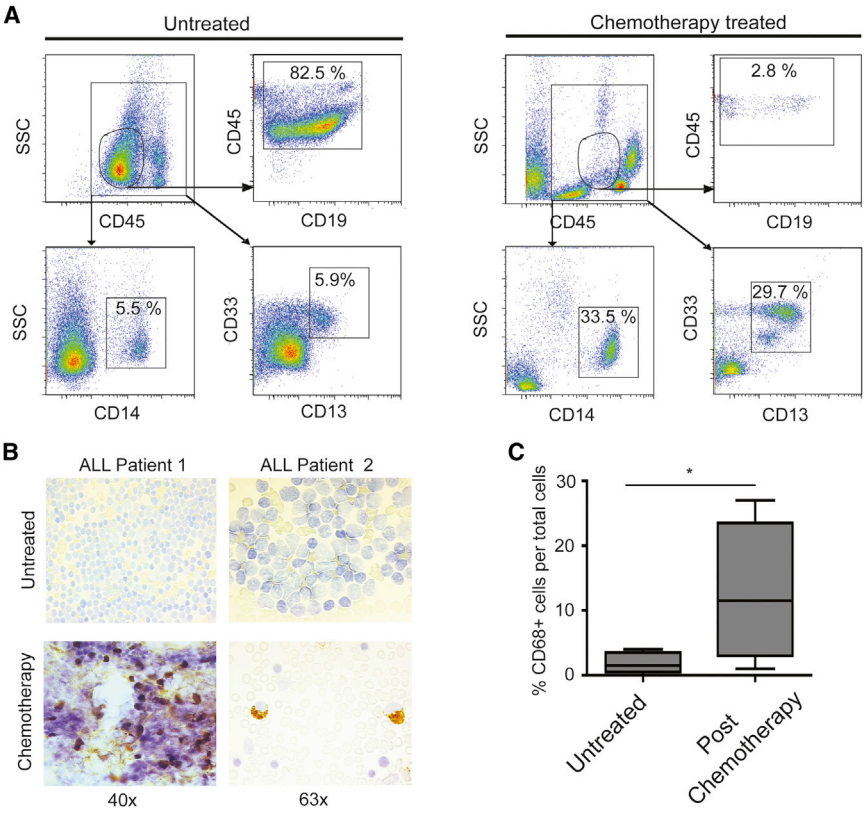

Figure 7. Polychemotherapy Induces Macrophage Infiltration in ALL Patients

(A) Flow cytometry assessment of bone marrow aspirates taken from a patient at diagnosis (left) and undergoing CTX-containing polychemotherapy (GMALL Induction I) at day 11 posttreatment start (right). The circular $CD45^+/CD19^+$ gate shows the number of lymphocytic blasts. In the rectangular $CD45^+$ gate, the $CD14^+$ and $CD13^+/CD33^+$ cells demarcate the bone marrow macrophage populations.

(B) Representative immunostaining for CD68 in bone marrow smears prior therapy (top) and at day 11 posttherapy onset (bottom).

(C) A graph showing the percentage of $CD68^+$ macrophages per total cells in bone marrow smears from 6 ALL patients prior to therapy and at day 11 of the first treatment cycle (* = $p < 0.05$).

chemotherapeutics with therapies involving monoclonal human-specific antibodies. While such regimens have been shown to improve patient outcome, the mechanism(s) underlying therapeutic synergy have not been elucidated. In this study, we examined treatment modalities that enhance alemtuzumab efficacy in drug refractory tumor microenvironments. While most antibody/drug combinations yielded only minor improvements in overall response, the combination of alemtuzumab with CTX resulted in a dramatic synergistic effect. Notably, CTX has previously been shown to enhance rituximab efficacy in the treatment of chronic lymphocytic leukemia (Keating et al., 2005; Tam et al., 2008). This combination also effectively eradicated the tumor burden in the bone marrow and yielded a long-term curative approach with no relapse of disease. Remarkably, we could systematically reduce the normal dose of CTX and still achieve maximal synergy with antibody therapy, suggesting that induction of tumor cell apoptosis by DNA damage is not the primary mechanism of action of CTX in this model. Rather, the synergistic effect of CTX relies on its ability to transform a protective microenvironment into one that is receptive to antibody therapy. Several mechanisms contribute to this "resensitization" of tumor cells in a protected microenvironment: CTX (1) reduces the overall disease burden and allows for an improved effector-target cell ratio, (2) inhibits secretion of PGE2, and most importantly, (3) induces a strong secretory response to improve macrophage activity. These processes have the combined effect of repopulating and activating monocytes in the bone marrow.

Notably, while CTX did induce changes on the surface of leukemic cells, the CTX-induced secretory crosstalk between leukemia cells and their microenvironment is the major contributor to antibody efficacy. This acute secretory activation phenotype (ASAP) response shows a maximum peak of cytokine release within 24 hr of treatment. This short window of cytokine release is consistent with the transient susceptibility of tumor cells to antibody-dependent killing. Specifically, we identified a narrow window of ±24 hr of codosing CTX and alemtuzumab, during which we could achieve a synergistic response. Importantly, we could identify strong CTX/antibody synergy for independent clinically established therapeutic antibodies in multiple preclinical leukemia models. These data provide important practical implications for current chemoimmunotherapy protocols like R-CHOP and FCR. Most of these regimens apply the therapeutic antibody prior to the application of CTX and additional genotoxic drugs (Hallek et al., 2010). Our data suggest that pretreatment of leukemias shortly before antibody administration is necessary to yield optimal effects. Our results also suggest that pretreatment with chemotherapy may allow for effective synergy at lower drug doses, suggesting a rational path toward dose reduction and reduced toxicity.

Recent studies have suggested that targeted agents can promote the efficacy of front-line chemotherapies. For example, normalization of the pancreatic tumor vasculature following treatment with hedgehog inhibitors can promote doxorubicin access to tumor cells (Olive et al., 2009). Our data present the opposite paradigm: that conventional chemotherapy can remodel the tumor microenvironment and potentiate the action of a targeted therapeutic. This effect of CTX treatment is highly specific and independent of its putative tumor debulking effect. Thus, we propose that the DNA-damage induced acute secretory activating phenotype (ASAP) of effector cells is the major synergistic mechanism of chemoimmunotherapy. We believe new clinical protocols that are optimized based on the temporal

kinetics of this secretory response will yield highly synergistic combinatorial regimens involving both existing and new clinical antibodies.

EXPERIMENTAL PROCEDURES

Generation of the PreB-ALL Model

Human hematopoietic stem cells were isolated from healthy donor cord blood using $CD133^+$-positive selection and expanded in vitro. After infection with the lentiviral CD19-promotor/Eμ-enhancer GFP-MYC-BCL2-construct, cells were injected into sublethally irradiated NOD-*scid Il2rg*$^{-/-}$ (NSG) mice and monitored for disease onset by counting the number of GFP^+ cells in the peripheral blood. Secondary NSGrecipient mice were injected with 10^6 cells derived from spleens of primary leukemic mice.

Antibody Therapy

Clinical-grade alemtuzumab (Genzyme) was obtained at a concentration of 30 mg/ml in sterile PBS and stored at 4°C until needed. Rituximab was obtained from Roche and applied 10 mg/ml. These compounds were then administered via tail vein injection at 5 μl/g mouse body weight. For inhibition of TNFα and VEGF in vivo, therapeutic antibodies specific for human TNFα (infliximab) and VEGF (bevacizuamb) were used in order to abrogate leukemia-cell-derived cytokines in vivo. Antibodies were injected at 30 mg/kg 24 hr prior to CTX injection, and injections were repeated at day 0 and at day 1 posttreatment. Organ response was assessed 7 days after chemoimmunotherapy onset as described above.

Isolation of Macrophages for the Antibody-Dependent Cellular Cytotoxicity Assay

Peritoneal macrophages were harvested by thioglycollate injection and peritoneal lavage. For macrophage ADCC, 10^5 cells per well were used at an effector to target ratio of 1:1. Antibody-specific killing was determined as % specific killing = 100 − (100*(total GFP^+ cells treated/total GFP^+ cells untreated)). Recombinant cytokines were purchased from Peprotech and used at 100 ng/ml. Blocking antibodies were applied to conditioned media 1 hr at 37°C at 10 μg/ml.

In Vivo RNAi-Screening Approach

An 88 shRNA containing library was generated based on predictions from siRNA Scales (Matveeva et al., 2007) and RNAi central (http://katahdin.cshl.edu). Oligonucleotides were synthesized individually and batch amplified and cloned into our previously published MLS retroviral vector carrying mCherry. 10^6 retrovirally infected $mCherry^+$ cells were injected into recipient mice and treatment with alemtuzumab initialized as described above at day 21 posttransplant. Leukemia cells were isolated from spleens at relapse, and high-throughput sequencing for representation of shRNA-pools was carried out after PCR-based amplification of shRNAs from genomic DNA.

Statistical Analysis

Statistical analysis was carried out using Excel, Prism GraphPad, and Matlab software packages applying Student's t test or Mann-Whitney *U* test. Log rank test was applied for survival analysis.

SUPPLEMENTAL INFORMATION

Supplemental Information includes Extended Experimental Procedures six figures, three tables, and one movie and can be found with this article online at http://dx.doi.org/10.1016/j.cell.2013.12.041.

ACKNOWLEDGMENTS

We thank Holly Criscione for expert technical assistance and Ryan Hayman for operational support. We also thank P. Bak, H. Eisen, and the entire Hemann lab for helpful discussions; the Swanson Biotechnology Center for excellent technical support; and J. Pritchard and L. Gilbert for critical reading of this manuscript. This work was partly supported by grants from the MIT Ludwig Center for Molecular Oncology (to M.T.H.), the Marble Family Foundation (to J.C. and M.T.H.), the National Research Foundation Singapore through the Singapore-MIT Alliance for Research and Technology's Interdisciplinary Research Group in Infectious Disease research program (to J.C.), and the German Research Foundation (DFG) as part of the KFO286 (to C.P.P., K.A.K., and M.H) and CRC832 (to L.H. and M.H). C.P.P. was supported by a research fellowship of the German Research foundation. This work was also supported in part by the Koch Institute Support (core) Grant P30-CA14051 from the National Cancer Institute.

Received: December 15, 2012
Revised: August 13, 2013
Accepted: December 30, 2013
Published: January 30, 2014

REFERENCES

Aukema, S.M., Siebert, R., Schuuring, E., van Imhoff, G.W., Kluin-Nelemans, H.C., Boerma, E.J., and Kluin, P.M. (2011). Double-hit B-cell lymphomas. Blood *117*, 2319–2331.

Chao, M.P., Alizadeh, A.A., Tang, C., Myklebust, J.H., Varghese, B., Gill, S., Jan, M., Cha, A.C., Chan, C.K., Tan, B.T., et al. (2010). Anti-CD47 antibody synergizes with rituximab to promote phagocytosis and eradicate non-Hodgkin lymphoma. Cell *142*, 699–713.

Chao, M.P., Alizadeh, A.A., Tang, C., Jan, M., Weissman-Tsukamoto, R., Zhao, F., Park, C.Y., Weissman, I.L., and Majeti, R. (2011). Therapeutic antibody targeting of CD47 eliminates human acute lymphoblastic leukemia. Cancer Res. *71*, 1374–1384.

Chen, Q., Zhang, X.H., and Massagué, J. (2011). Macrophage binding to receptor VCAM-1 transmits survival signals in breast cancer cells that invade the lungs. Cancer Cell *20*, 538–549.

Clynes, R.A., Towers, T.L., Presta, L.G., and Ravetch, J.V. (2000). Inhibitory Fc receptors modulate in vivo cytotoxicity against tumor targets. Nat. Med. *6*, 443–446.

Coiffier, B., Lepage, E., Briere, J., Herbrecht, R., Tilly, H., Bouabdallah, R., Morel, P., Van Den Neste, E., Salles, G., Gaulard, P., et al. (2002). CHOP chemotherapy plus rituximab compared with CHOP alone in elderly patients with diffuse large-B-cell lymphoma. N. Engl. J. Med. *346*, 235–242.

DeNardo, D.G., Barreto, J.B., Andreu, P., Vasquez, L., Tawfik, D., Kolhatkar, N., and Coussens, L.M. (2009). CD4(+) T cells regulate pulmonary metastasis of mammary carcinomas by enhancing protumor properties of macrophages. Cancer Cell *16*, 91–102.

DeNardo, D.G., Brennan, D.J., Rexhepaj, E., Ruffell, B., Shiao, S.L., Madden, S.F., Gallagher, W.M., Wadhwani, N., Keil, S.D., Junaid, S.A., et al. (2011). Leukocyte complexity predicts breast cancer survival and functionally regulates response to chemotherapy. Cancer Discov. *1*, 54–67.

Dougan, M., and Dranoff, G. (2009). Immune therapy for cancer. Annu. Rev. Immunol. *27*, 83–117.

Fan, Z., Baselga, J., Masui, H., and Mendelsohn, J. (1993). Antitumor effect of anti-epidermal growth factor receptor monoclonal antibodies plus cis-diamminedichloroplatinum on well established A431 cell xenografts. Cancer Res. *53*, 4637–4642.

Gökbuget, N., Raff, R., Brügge-Mann, M., Flohr, T., Scheuring, U., Pfeifer, H., Bartram, C.R., Kneba, M., and Hoelzer, D. (2004). Risk/MRD adapted GMALL trials in adult ALL. Ann. Hematol. *83* (*Suppl 1*), S129–S131.

Hallek, M., Fischer, K., Fingerle-Rowson, G., Fink, A.M., Busch, R., Mayer, J., Hensel, M., Hopfinger, G., Hess, G., von Grünhagen, U., et al.; International Group of Investigators; German Chronic Lymphocytic Leukaemia Study Group (2010). Addition of rituximab to fludarabine and cyclophosphamide in patients with chronic lymphocytic leukaemia: a randomised, open-label, phase 3 trial. Lancet *376*, 1164–1174.

Harris, S.G., Padilla, J., Koumas, L., Ray, D., and Phipps, R.P. (2002). Prostaglandins as modulators of immunity. Trends Immunol. *23*, 144–150.

Jackson, S.H., Gallin, J.I., and Holland, S.M. (1995). The p47phox mouse knock-out model of chronic granulomatous disease. J. Exp. Med. *182*, 751–758.

Jaiswal, S., Chao, M.P., Majeti, R., and Weissman, I.L. (2010). Macrophages as mediators of tumor immunosurveillance. Trends Immunol. *31*, 212–219.

Keating, M.J., O'Brien, S., Albitar, M., Lerner, S., Plunkett, W., Giles, F., Andreeff, M., Cortes, J., Faderl, S., Thomas, D., et al. (2005). Early results of a chemoimmunotherapy regimen of fludarabine, cyclophosphamide, and rituximab as initial therapy for chronic lymphocytic leukemia. J. Clin. Oncol. *23*, 4079–4088.

Leskov, I., Pallasch, C.P., Drake, A., Iliopoulou, B.P., Souza, A., Shen, C.H., Schweighofer, C.D., Abruzzo, L., Frenzel, L.P., Wendtner, C.M., et al. (2013). Rapid generation of human B-cell lymphomas via combined expression of Myc and Bcl2 and their use as a preclinical model for biological therapies. Oncogene *32*, 1066–1072.

Lim, S.H., Vaughan, A.T., Ashton-Key, M., Williams, E.L., Dixon, S.V., Chan, H.T., Beers, S.A., French, R.R., Cox, K.L., Davies, A.J., et al. (2011). Fc gamma receptor IIb on target B cells promotes rituximab internalization and reduces clinical efficacy. Blood *118*, 2530–2540.

Matveeva, O., Nechipurenko, Y., Rossi, L., Moore, B., Saetrom, P., Ogurtsov, A.Y., Atkins, J.F., and Shabalina, S.A. (2007). Comparison of approaches for rational siRNA design leading to a new efficient and transparent method. Nucleic Acids Res. *35*, e63.

Meacham, C.E., Ho, E.E., Dubrovsky, E., Gertler, F.B., and Hemann, M.T. (2009). In vivo RNAi screening identifies regulators of actin dynamics as key determinants of lymphoma progression. Nat. Genet. *41*, 1133–1137.

Meyer, L.H., Eckhoff, S.M., Queudeville, M., Kraus, J.M., Giordan, M., Stursberg, J., Zangrando, A., Vendramini, E., Möricke, A., Zimmermann, M., et al. (2011). Early relapse in ALL is identified by time to leukemia in NOD/SCID mice and is characterized by a gene signature involving survival pathways. Cancer Cell *19*, 206–217.

Minard-Colin, V., Xiu, Y., Poe, J.C., Horikawa, M., Magro, C.M., Hamaguchi, Y., Haas, K.M., and Tedder, T.F. (2008). Lymphoma depletion during CD20 immunotherapy in mice is mediated by macrophage FcgammaRI, FcgammaRIII, and FcgammaRIV. Blood *112*, 1205–1213.

Molina, A. (2008). A decade of rituximab: improving survival outcomes in non-Hodgkin's lymphoma. Annu. Rev. Med. *59*, 237–250.

Moreton, P., and Hillmen, P. (2003). Alemtuzumab therapy in B-cell lymphoproliferative disorders. Semin. Oncol. *30*, 493–501.

Olive, K.P., Jacobetz, M.A., Davidson, C.J., Gopinathan, A., McIntyre, D., Honess, D., Madhu, B., Goldgraben, M.A., Caldwell, M.E., Allard, D., et al. (2009). Inhibition of Hedgehog signaling enhances delivery of chemotherapy in a mouse model of pancreatic cancer. Science *324*, 1457–1461.

Sausville, E.A., and Burger, A.M. (2006). Contributions of human tumor xenografts to anticancer drug development. Cancer Res. *66*, 3351–3354, discussion 3354.

Shinomiya, S., Naraba, H., Ueno, A., Utsunomiya, I., Maruyama, T., Ohuchida, S., Ushikubi, F., Yuki, K., Narumiya, S., Sugimoto, Y., et al. (2001). Regulation of TNFalpha and interleukin-10 production by prostaglandins I(2) and E(2): studies with prostaglandin receptor-deficient mice and prostaglandin E-receptor subtype-selective synthetic agonists. Biochem. Pharmacol. *61*, 1153–1160.

Tam, C.S., O'Brien, S., Wierda, W., Kantarjian, H., Wen, S., Do, K.A., Thomas, D.A., Cortes, J., Lerner, S., and Keating, M.J. (2008). Long-term results of the fludarabine, cyclophosphamide, and rituximab regimen as initial therapy of chronic lymphocytic leukemia. Blood *112*, 975–980.

Wendtner, C.M., Ritgen, M., Schweighofer, C.D., Fingerle-Rowson, G., Campe, H., Jäger, G., Eichhorst, B., Busch, R., Diem, H., Engert, A., et al.; German CLL Study Group (GCLLSG) (2004). Consolidation with alemtuzumab in patients with chronic lymphocytic leukemia (CLL) in first remission—experience on safety and efficacy within a randomized multicenter phase III trial of the German CLL Study Group (GCLLSG). Leukemia *18*, 1093–1101.

Williams, C.S., Tsujii, M., Reese, J., Dey, S.K., and DuBois, R.N. (2000). Host cyclooxygenase-2 modulates carcinoma growth. J. Clin. Invest. *105*, 1589–1594.